Physica Scripta

PAPER

On two-parameter bifurcation and analog circuit implementation of a Chameleon chaotic system

RECEIVED
27 September 2023

REVISED
19 November 2023

ACCEPTED FOR PUBLICATION
4 December 2023

PUBLISHED
13 December 2023

Weiwei Fan, Dan Xu, Zhiyin Chen, Ning Wang and Quan Xu*

School of Microelectronics and Control Engineering, Changzhou University, Changzhou 213159, People's Republic of China
* Author to whom any correspondence should be addressed.

E-mail: xuquan@cczu.edu.cn

Keywords: Chameleon chaotic system, two-dimensional bifurcation, hidden oscillation, basin of attraction, analog circuit implementation

Abstract

In this paper, the two-parameter space bifurcation of a three-dimensional Chameleon system is investigated. It is called Chameleon since the type and the number of the system equilibrium are adjustable for different parameter configurations. Aided by the computation analysis, the graphic structures of two-parameter bifurcation of the Chameleon system are characterized for the first time. With different two-parameter configurations, the bifurcation evolution shows that various self-excited and hidden attractors exist. In addition, numerical demonstration of the two-dimensional slice through the attraction basin space is presented. The results show that the basin of attraction of the typical hidden chaotic attractor does not associated with the origin, which makes the attractor difficult to be numerically localized and experimentally observed. To solve the problem, offset boost scheme is adopted to control the basin of attraction and make it touch the origin, which allows to coin the hidden attractor via configuring zero initial value and making it feasible in experimental observation. Finally, the analog circuit-assisted experiment validated the feasibility of the scheme.

1. Introduction

Since the discovery of the butterfly effect in nonlinear system, the research on chaotic oscillations and chaos mechanism has become a hotspot [1–3]. For most autonomous ordinary differential equations (ODE) chaotic systems, the chaotic motions can be triggered by choosing an initial point in the small neighborhood of the systems' unstable equilibrium (if exists) since these motions are common self-excited oscillations [4–6]. The generated attractors in these systems usually have relatively large basins of attraction wrapping up at least one unstable equilibrium, such as the scroll-type Chua's attractor [7–9], the butterfly-type Lorenz attractor [10–12], and many other chaotic attractors in various nonlinear circuits and systems [13–15]. In recent decade, with the birth of the theory of hidden attractors and hidden oscillations [16–18], some relatively new hidden oscillating systems have attracted special interest [19–21]. An attractor is called hidden attractor when its basin of attraction is not intersected with the system equilibrium [22–24]. With this condition, it is difficult to trigger such attractor via configuring an initial point from the small neighborhood of the system equilibrium. In various cases, the one with no equilibrium is a natural hidden oscillating system since the existence of the attractor is not related to the system equilibrium [25], which makes it have advantages in resisting the prediction of chaotic trajectories in chaos-based security applications [26].

Before the 2010s, more attention has been paid to the chaotic systems with unstable equilibrium. These attractors are self-excited since the basins of attractors intersect with the system equilibria, which allows us to calculate the system trajectories from the neighborhoods of equilibria using a standard calculation program to obtain the self-excited attractor [27, 28]. However, the emergence of the concept of hidden attractor makes the chaotic system with no equilibrium receive new attention since the absent equilibrium cannot provide any valuable information for locating the phase space trajectories [29, 30]. Inspired by the Sprott-D system [31], Wei proposed a three-dimensional autonomous system with no equilibrium [32], which provides an active

© 2023 IOP Publishing Ltd

promotion for designing more interesting chaotic systems with no equilibrium. After that, some new cases of chaotic systems with no equilibrium were reported one after another. Sajad *et al* presented a variety of 3-D simple chaotic flows with no equilibrium [33]. Some no-equilibrium chaotic systems with multi-structure attractors were designed as well [34–36].

The Chameleon chaotic system is a unique system which has different kinds of equilibria or has no equilibrium for different parameter configurations. Consequently, it yields different self-excited and hidden attractors [37, 38]. Wei system is a widely studied dynamical system with complex self-excited and hidden oscillations [32]. This system is a Chameleon system as it has different numbers of equilibria or has no equilibrium with the variation of parameters. When the system has no equilibrium, the hidden oscillations are generated. For examination of the potential long-duration transient or the sound steady state, some important points such as the step size of the integrator and the total time length should be carefully taken into consideration in numerical computation [39, 40], which usually leads to misjudge of the transient attractor. Taking another way, these issues can be greatly weakened in analog circuit-based experimental examinations as the resistor-capacitor integrator emulating a continuous-time reverse-process for operation of ODE systems [41].

In terms of the experimental examination of the hidden attractors, the digital circuit implementation based on the discretized ODE systems [42] and the analog circuit implementation based on the continuous resistor-capacitor integrator [43] are typically used. Firstly, maintaining the consistency of the step size with numerical simulations, the high clock frequency of the digital processing platform sustains the discretized ODE systems iterate in a sufficient large time length [44]. Secondly, the continuous resistor-capacitor integrator in analog circuit completely avoids the discretization effect and ensures the continuous operation in relatively large time scale of the physical sense. However, the explicit examination via physical experiments remains a rather under-investigated topic in the Chameleon system with hidden dynamics. To this purpose, this paper makes the following three main contributions.

- We numerically detect the evolution route and boundary of the Chameleon chaotic system using two-dimensional bifurcation analyses.
- In order to enhance the feasibility of experimental implementation of the Chameleon chaotic system, we further apply an offset boost approach to make the basin of attraction of the hidden attractor intersect with the origin.
- We finally present the resistor-capacitor integrator-based analog circuit implementation of the Chameleon chaotic system, which allows one to reliably examine the system dynamics to be the steady hidden oscillating state.

The remaining parts are as follows. Section 2 proposes some basic analyses of the Chameleon chaotic system. In Section 3, the route to chaos and the evolution boundary are numerically detected using two-dimensional bifurcation analyses. The attraction basin analyses and analog circuit experiment are presented in Section 4. The last section provides some conclusions of this paper.

2. A chameleon chaotic system

In this section, different types of system equilibria under different parameter configurations are discussed. A typical hidden oscillating chaotic attractor is numerically demonstrated.

2.1. System model

By adding a coefficient c to the term x of the second equation and a constant perturbation d to the third equation of the following Sprott-D system [31],

$$\begin{aligned} \dot{x} &= -y, \\ \dot{y} &= x + z, \\ \dot{z} &= ay^2 + xz, \end{aligned} \tag{1}$$

Wei proposed a three-dimensional autonomous system [32]

$$\begin{aligned} \dot{x} &= -y, \\ \dot{y} &= cx + z, \\ \dot{z} &= ay^2 + xz - d, \end{aligned} \tag{2}$$

where a, c, and d are three system parameters. Due to the existence of different types of equilibria and complex chaotic dynamical behaviors, this system is regarded as a Chameleon chaotic system. The details of the types of equilibria under different parameter configurations are presented as follows.

By solving $\dot{x} = 0$, $\dot{y} = 0$, and $\dot{z} = 0$, the equilibrium point E^*: (x^*, y^*, z^*) (if exists) of system (2) can be obtained. Jacobian of linearization of system (2) at equilibria E^* is

$$\mathbf{J}(E^*) = \begin{pmatrix} 0 & -1 & 0 \\ c & 0 & 1 \\ z^* & 2ay^* & x^* \end{pmatrix}. \tag{3}$$

The corresponding characteristic equation at E^* is

$$P(\lambda) = \det(1\lambda - \mathbf{J}(E^*)) = \lambda^3 + a_1\lambda^2 + a_2\lambda + a_3 = 0, \tag{4}$$

where

$$a_1 = -x^*,\ a_2 = c - 2ay^*,\ a_3 = -cx^* + z^*. \tag{5}$$

According to the Routh–Hurwitz criterion, E^* is asymptotically stable when the real parts of all roots λ are negative if and only if

$$a_1 > 0,\ a_3 > 0,\ a_1a_2 - a_3 > 0. \tag{6}$$

2.2. System equilibrium

System (2) has different numbers of equilibria or no equilibria for different parameter configurations. Three cases are given as follows.

(i) When $cd < 0$, system (2) has two equilibria

$$E_1^*: \left(\sqrt{-\frac{d}{c}},\ 0,\ -\sqrt{-cd}\right),\ E_2^*: \left(-\sqrt{-\frac{d}{c}},\ 0,\ \sqrt{-cd}\right). \tag{7}$$

(ii) When $c \neq 0$ and $d = 0$, system (2) has only one equilibrium point at the origin O, i.e.,

$$E_0^*: (0,\ 0,\ 0). \tag{8}$$

(iii) When $cd > 0$, system (2) has no equilibria, i.e.,

$$E^* = \varnothing. \tag{9}$$

Besides, for one of the following parameter configurations

(i) $c = 0$ and $d = 0$,

(ii) $(a + 1)c < 0$ and $d = 0$,

(iii) $(a + 1)d < 0$ and $c = 0$,

(iv) $a \leqslant -1, c > 0$, and $d > 0$,

(v) $a \geqslant -1, c < 0$, and $d < 0$,

system (2) does not have bound chaotic solutions, which can be proved through that equation (2) integrates to

$$x'' + cx - xx' = \int_0^t [d + cx^2 - (a + 1)x'^2] + C. \tag{10}$$

Under parameter configurations (i)–(v), (10) has a monotone left-hand side. Thus when the time t tends to infinity, the time-related polynomial $xy - z$ has a limit $L \in \overline{R}$. If L is finite, then any attractor (if exists) for the system (2) lies on the surface $xy - z$ and will not be chaotic. When $L = \pm\infty$, there exists at least one state variable that is not bounded and coins divergence.

We further discuss the stability of the equilibrium for different parameter configurations, mainly contains the following three cases, i.e., (i) $cd < 0$, (ii) $c \neq 0$ and $d = 0$, (iii) $cd > 0$.

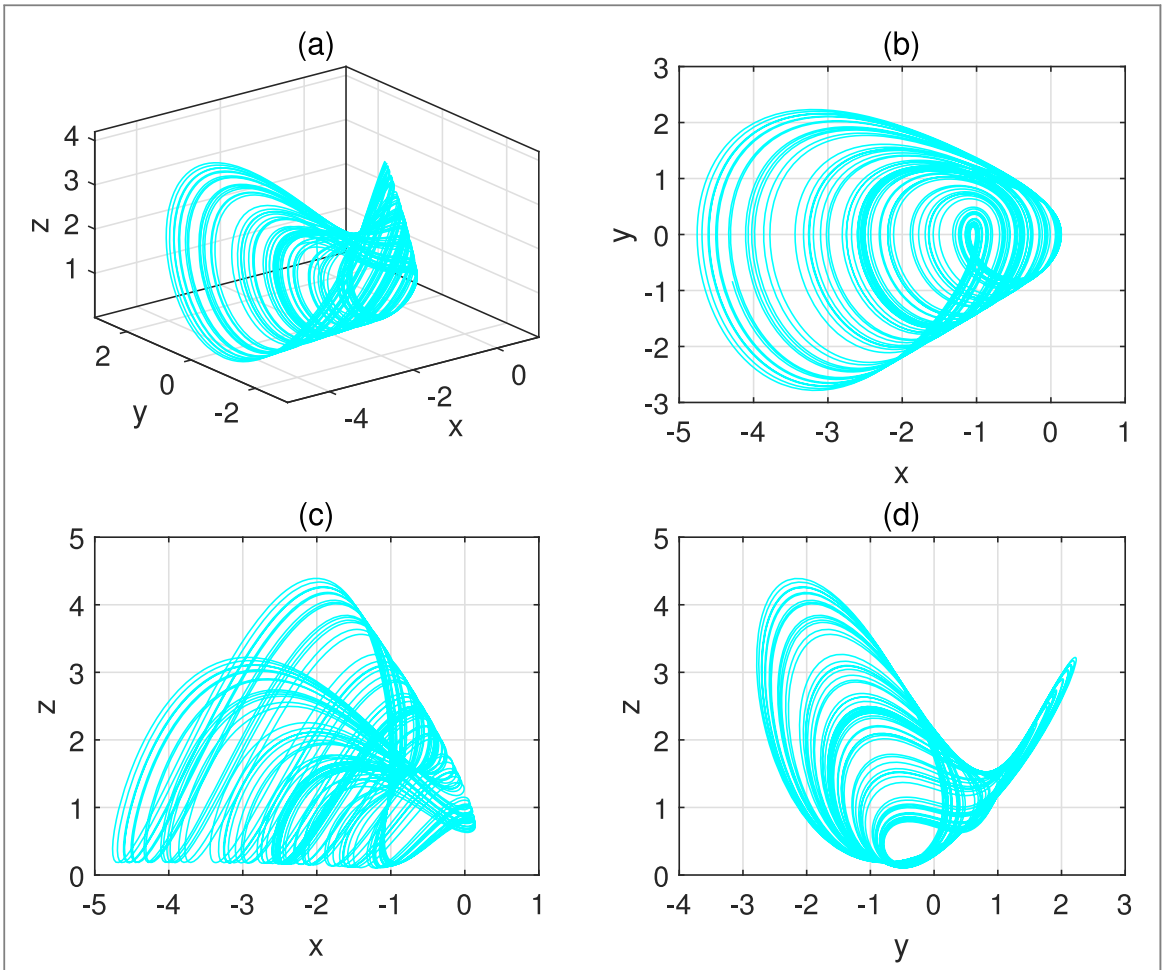

Figure 1. The phase portraits of system (2) for the parameter configurations $a = 2$, $c = 1$, and d=0.35, and the initial values ($x(0)$, $y(0)$, $z(0)$) = (0, 0, 1): (a) the trajectory in 3-D space; (b) the projection in $x - y$ plane; (c) the projection in $x - z$ plane; (d) the projection in $y - z$ plane.

2.2.1. Case of cd < 0

For the first case of $cd < 0$, system (2) has two symmetric equilibria $E_{1,2}^*$ as listed in (7).

In the equilibrium point E_1^*, the three coefficients of the characteristic equation (4) are

$$a_1 = -\sqrt{-\frac{d}{c}},\ a_2 = c,\ a_3 = -c\sqrt{-\frac{d}{c}} - \sqrt{-cd}. \tag{11}$$

It is obvious that $a_1 < 0$, the first inequality of the criterion (6) is not satisfied, and thus the equilibrium point E_1^* is not asymptotically stable.

Similarly, in the equilibrium point E_2^*, we obtain the three coefficients of equation (4)

$$a_1 = \sqrt{-\frac{d}{c}},\ a_2 = c,\ a_3 = c\sqrt{-\frac{d}{c}} + \sqrt{-cd}. \tag{12}$$

Due to $a_1 a_2 - a_3 = -\sqrt{-cd} < 0$, the third inequality of the criterion (6) is not satisfied, thus E_2^* is not asymptotically stable as well.

2.2.2. Case of c $\neq 0$ *and* $d = 0$

For the second case of $c \neq 0$ and $d = 0$, system (2) has only one equilibrium point E_0^*: (0, 0, 0) at the origin O. In the equilibrium point E_0^*, the three coefficients of the characteristic equation (4) are

$$a_1 = 0,\ a_2 = c,\ a_3 = 0. \tag{13}$$

It is obvious that all inequalities in (6) are not satisfied, indicating E_0^* is not asymptotically stable. In specific, if $c > 0$ and $d = 0$, E_0^* is non-hyperbolic as the eigenvalues of the Jacobian of the linearized system are $\lambda_1 = 0$ and $\lambda_{2,3} = \pm\sqrt{c}\,i$. When $c < 0$ and $d = 0$, E_0^* is unstable as the eigenvalues of the Jacobian of the linearized system are $\lambda_1 = 0$ and $\lambda_{2,3} = \pm\sqrt{-c}$.

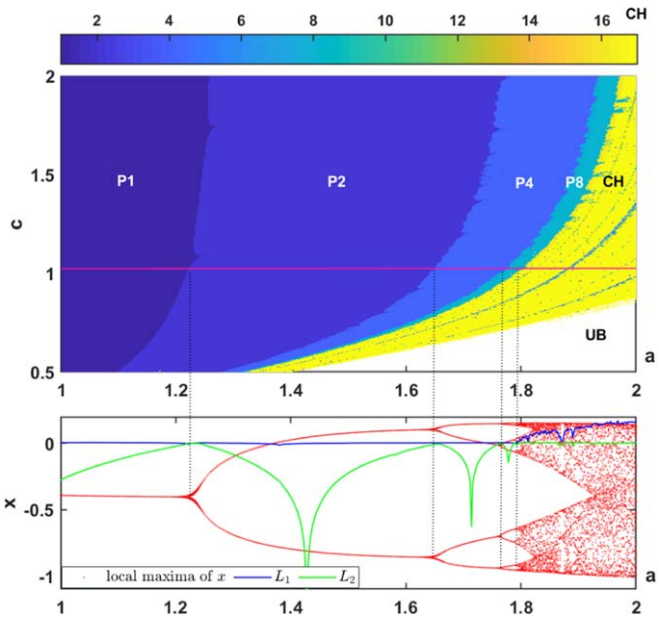

Figure 2. Bifurcation with respect to the parameters a and c, where $d = 0.35$, the upper panel plots the two-parameter bifurcation in the area $a \times c = [1, 2] \times [0.5, 2]$, the lower panel shows a specific case of the single-parameter bifurcation for $a \in [1, 2]$, $c = 1$, and d=0.35.

2.2.3. Case of cd $>$ *0*

For the third case of $cd > 0$, system (2) has no equilibria.

2.3. Phase plot

Furthermore, the fourth-order Runge-Kutta algorithm is used to carry out numerical simulations, where the time-step and the time-length are 0.01 and 400, respectively. When the specific parameters $a = 2, c = 1, d$=0.35 and the initial values $(x(0), y(0), z(0)) = (0, 0, 1)$ are configured, the phase portraits of system (2) are plotted in figure 1. By using Wolf's algorithm [45], the three Lyapunov exponents are calculated as L_1=0.174, $L_2 \approx 0$, and $L_3 = -3.031$. According to the three exponents, the corresponding Kaplan-York dimension is obtained as $D_{KY} \approx 2.057$. The results $L_1 > 0$ and $2 < D_{KY} < 3$ indicate that the trajectory of the attractor is chaotic.

3. Two-parameter bifurcation and route to chaos

In this section, aided by computation analysis, the graphic structures of two-parameter bifurcations of the Chameleon chaotic system are characterized. In [32], the dynamical behaviors of system (2) were investigated using phase plots, Poincaré mapping, single-parameter Lyapunov exponents, and single-parameter bifurcation diagram. Note that for a given system with two or more parameters, it is difficult to present a comprehensive dynamics study using single-parameter analysis. Especially for system (2) with three parameters, it is better to explore the two-parameter space to completely characterize various dynamical behaviors, bifurcation boundaries that separate them, and the divergence space. To keep consistence with the original Wei system, we here consider the parameter space $(a, c, d) \in \Omega = \{(a, c, d) | a > 0, c > 0, d > 0\}$ to carry out a detailed two-parameter dynamics analysis.

3.1. Bifurcation in the $a - c$ parameter plane

We first take the $a - c$ parameter plane into consideration and present the bifurcation diagram analysis. For $d = 0.35$, the two-parameter area $a \times c = [1, 2] \times [0.5, 2]$ is chosen to exhibit the rich dynamics, as shown in the upper panel of figure 2, in which the color bar marks the periodicity of the system trajectory that is counted by sampling the distinct peaks of the time sequences of the system variable x. It is found that system (2) undergoes a classical route to chaos of period-doubling bifurcation. In specific, with parameter a increasing from 1, the system evolutes from the period-1 (P1) limit cycle, and then goes to period-2 (P2) limit cycle, period-4 (P4) limit cycle, period-8 (P8) limit cycle, and finally generates chaotic (CH) motions. Besides, there exists a white area where the system orbits are tending to infinity and coin unbounded (UB) behavior.

For further demonstrating the period-doubling bifurcation route, we fix $c = 1, d = 0.35$, and increase a from 1 to 2, to plot a single-parameter bifurcation diagram in the lower panel of figure 2. It is shown that several

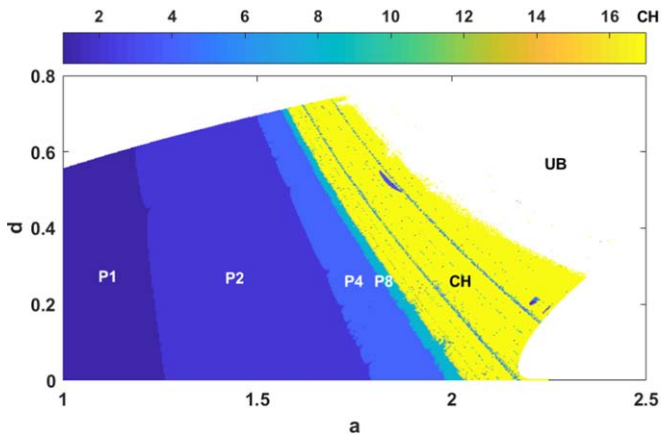

Figure 3. Bifurcation with respect to the parameters a and d, where $c = 1$, the periodicity of the system trajectory corresponds the number of the color bar and some identical states of period-1, period-2, period-4, period-8, chaos, and unbounded area are marked by P1, P2, P4, P8, CH, and UB, respectively.

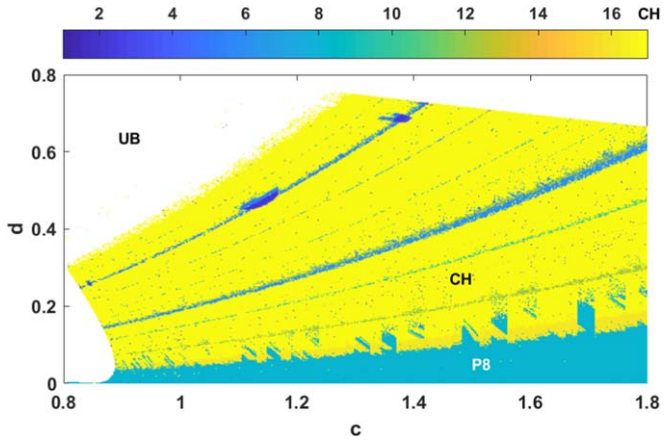

Figure 4. Bifurcation with respect to the parameters c and d, where $a = 2$, the periodicity of the system trajectory corresponds the number of the color bar and some identical states of period-8, chaos, and unbounded area are marked by P8, CH, and UB, respectively.

bifurcation points sequentially exist in $a = 1.222, 1.645, 1.768, 1.794$, and 1.798. For $a \in [1, 1.222]$, system (2) shows the period-1 attractor. After that, system (2) respectively generates the period-2, period-4, and period-8 attractors in the regions $a \in [1.222, 1.645]$, $[1.645, 1.768]$, and $[1.768, 1.794]$. With the further increase of a, period-16 attractors exist in a narrow region $[1.794, 1.798]$. Finally, chaos is generated in a wide region of $a \in [1.798, 2]$. The evolution of the system dynamics for $a \in [1, 2]$ demonstrates a classical period-doubling bifurcation route to chaos.

3.2. Bifurcation in the $a - d$ parameter plane

We then consider the $a - d$ parameter plane to demonstrate the two-parameter bifurcation diagram. For $c = 1$, the two-parameter area $a \times d = [1, 2.5] \times (0.001, 0.8]$ is chosen to exhibit the system dynamics, as shown in figure 3. Similarly, the periodicity of the system trajectory corresponds the number of the color bar and some identical states are marked by P1, P2, P4, P8, and CH. The evolution of the dynamics exhibits a classical period-doubling bifurcation route to chaos for increasing the parameter a. Besides, system (2) has a clear boundary between the unbounded motion area UB and the bounded ones of P1, P2, P4, P8, and CH, which is previously uncovered in this Chameleon chaotic system. Note that the above-mentioned dynamics are all related to the parameter a. For the third case that $cd > 0$ in section 2.2.3, system (2) will never have any equilibria. Therefore, we will finally demonstrate the hidden system dynamics in $c - d$ parameter plane.

3.3. Bifurcation in the $c - d$ parameter plane

Here, the $c - d$ parameter plane is taken as the last case to demonstrate the two-parameter bifurcation diagram. As for $cd > 0$, system (2) has no equilibria and the potential dynamics will be hidden. For $a = 2$ and

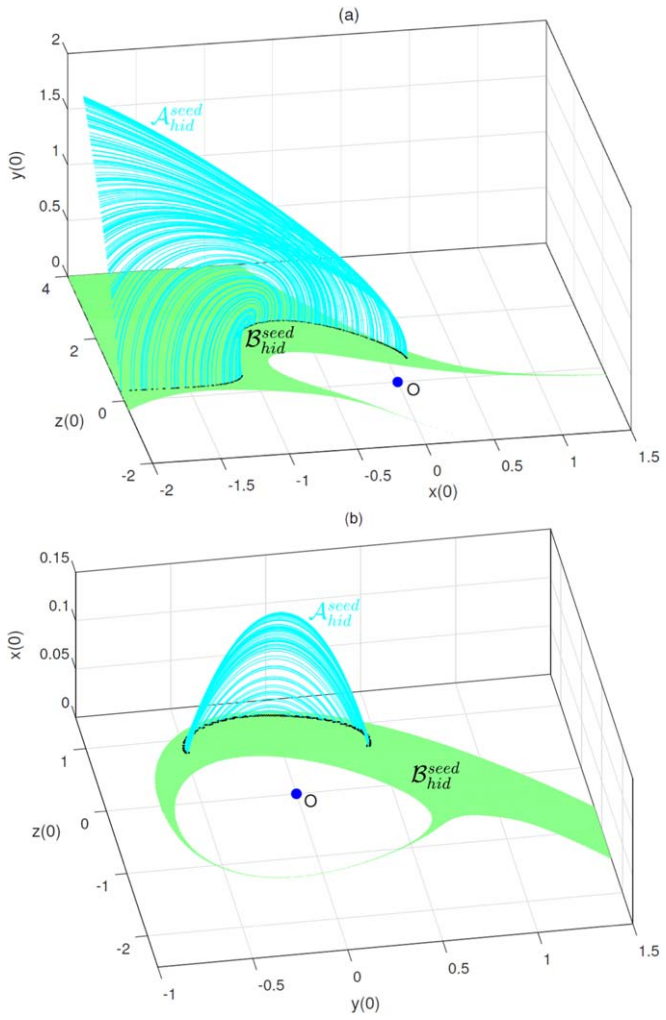

Figure 5. Basin of attraction of the hidden chaotic attractor in the section $x(0) - z(0)$ and $y(0) - z(0)$, where system (2) with a set of typical parameters $a = 2$, $c = 1$, and d=0.35 are used: (a) local basin in the $x(0) - z(0)$ plane and the local system trajectory in three-dimensional space; (b) local basin in the $y(0) - z(0)$ plane and the local system trajectory in three-dimensional space.

$c \times d = [0.8, 1.8] \times (0.001, 0.8]$, a two-parameter bifurcation diagram is exhibited in figure 4. In the chosen area, the system dynamics mainly show P8, P16, CH, and UB. All the generated bounded orbits in this area are hidden oscillating no matter what the value of a is. Besides, the boundary between the unbounded area UB and bounded ones with hidden oscillations are clearly investigated via the numerically plotted diagram, which provides an intuitive guidance for configuring the parameters c and d to obtain distinct hidden attractors from this Chameleon chaotic system.

4. Basin offset and experimental study

For chaotic system with no equilibrium, the experimental study is an important research topic as the hidden attractors are usually triggered by non-zero initial values. Take the system (2) with a set of typical parameters $a = 2$, $c = 1$, and $d = 0.35$ as an example, the hidden chaotic attractor is triggered by the non-zero initial values (IC) $(x(0), y(0), z(0)) = (0, 0, 1)$. In this section, we employ the offset control to shift the basin of attraction of the hidden chaotic attractor and make it intersect with the origin, which provides a solution for effective experimental detection of the hidden attractor. Meanwhile, an analog circuit-assisted experiment is presented, in which the hidden attractor is generated via pre-discharging all dynamic circuit elements to configure a set of experimentally available near-zero ICs.

4.1. Basin offset for configuring initial values

It has been recognized that the chaotic attractors generated from dynamical systems with no equilibrium are hidden as their basins of attraction will never intersect with the absent equilibrium. Thus, a hidden chaotic attractor can be generated from the system (2) with the configurations of parameters $a = 2$, $c = 1$, $d = 0.35$ and

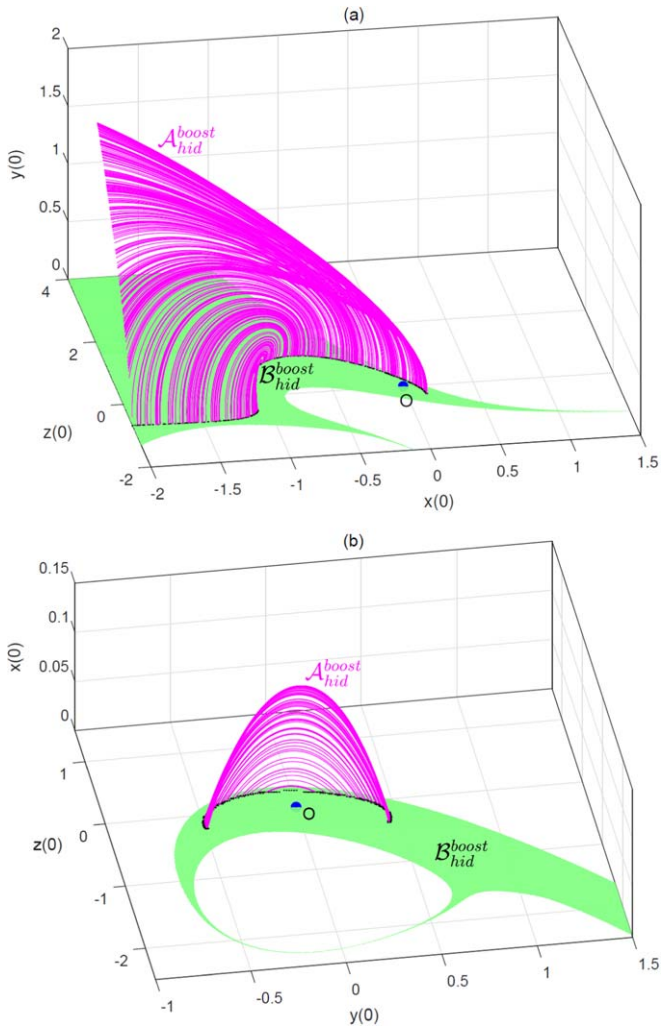

Figure 6. Basin of attraction of the hidden chaotic attractor in the section $x(0) - z(0)$ and $y(0) - z(0)$, where system (15) with a set of typical parameters $a = 2$, $c = 1$, $d = 0.35$, and $z_0 = 1$ are used: (a) local basin in the $x(0) - z(0)$ plane and the local system trajectory in three-dimensional space; (b) local basin in the $y(0) - z(0)$ plane and the local system trajectory in three-dimensional space.

the ICs (0, 0, 1). With this configuration, we first study the dynamics in the initial value space, i.e., the attraction basin visualisation [46]. The local basin of attraction and trajectory of the hidden chaotic attractor is numerically investigated as plotted in figure 5.

The results of figure 5(a) show the local slice of the attraction basin of the system (2), where the green basin $\mathcal{B}_{hid}^{seed}$ corresponds to the hidden chaotic attractor $\mathcal{A}_{hid}^{seed}$, the crossing trajectory in the section $y(0) = 0$ is marked by black. It is shown that the origin O is located at the unbounded space, which means that the starting orbits in a small space near O will not coin the hidden attractor $\mathcal{A}_{hid}^{seed}$. Or, to put it more straightforwardly, these starting orbits will quickly diverge to infinity. Similarly, figure 5(b) exhibits the local attraction basin and phase portraits of the hidden chaotic attractor generated from system (2), in which the IC set $\mathcal{B}_{hid}^{seed}$ for triggering the attractor $\mathcal{A}_{hid}^{seed}$ is not connected with the origin O as well. It means that the hidden chaotic attractor can only be generated via configuring non-zero ICs.

In practical electronic circuits, the charge of the dynamic capacitor element and holding it under a specific voltage are very difficult. In other words, it cannot ensure the initial state of the dynamic capacitor element is controllable when the whole circuit starts work, which makes it difficult to experimentally detect such hidden chaotic attractor. On the contrary, the discharge of the dynamic capacitor element to a near-zero voltage is relatively easy. But the prerequisites for using this method is that the basin of attraction of the hidden attractor is intersected with the origin.

Based on this consideration, in order to make it feasible to generate hidden chaotic attractor from an initial point at the origin, it is necessary to apply an offset boost via introducing a set of non-zero boosters with amplitudes x_0, y_0, and z_0 in the corresponding three directions, respectively. Here, $x_0 = 0$ and $y_0 = 0$ can be fixed, and the non-zero amplitude $z_0 = 1$ can be applied to implement an offset along the negative direction of

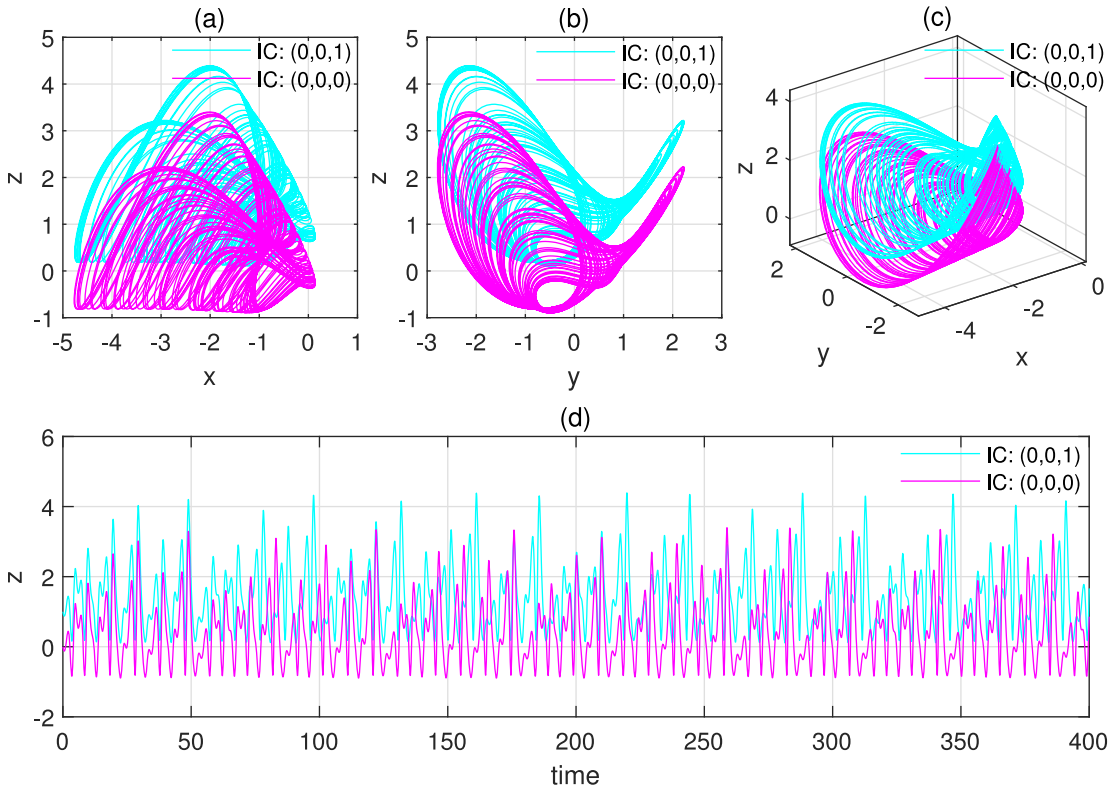

Figure 7. The phase portraits of systems (2) (cyan) and (15) (magenta) for the parameter configurations $a = 2, c = 1, d = 0.35$, and $z_0 = 1$, in which two sets of initial values (0, 0, 1) and (0, 0, 0) are respectively used for the two systems: (a) the projections in $x - z$ plane; (b) the projections in $y - z$ plane; (c) the trajectories in 3-D space; (d) the time sequences of the variable z.

z-axis, i.e., apply the variable transformation

$$(x, y, z) \rightarrow (x, y, z + z_0) \tag{14}$$

and obtain the following offset-boostable system

$$\begin{aligned} \dot{x} &= -y, \\ \dot{y} &= cx + (z + z_0), \\ \dot{z} &= ay^2 + x(z + z_0) - d. \end{aligned} \tag{15}$$

Furthermore, the local attraction basin in the section $y(0) = 0$ and the local 3-D phase portrait of the offset-boosted system (15) are plotted for comparison, as shown in figure 6(a). In contrary to the seed system (2), the boosted system (15) has a boosted hidden chaotic attractor $\mathcal{A}_{hid}^{boost}$ that can be generated via choosing initial point from $\mathcal{B}_{hid}^{boost}$. After boosting, the origin O is now involved in the basin of attraction $\mathcal{B}_{hid}^{boost}$, which indicates that the starting orbits near O will be able to coin the hidden attractor $\mathcal{A}_{hid}^{boost}$.

We further choose the section $x(0) = 0$ to study the attraction basin in the local areas of $y(0) \times z(0) \in [-1, 1.5] \times [-2.5, 1.5]$, as shown in figure 6(b). Similarly, in comparison with figure 5(b), only the location of the hidden chaotic attractor $\mathcal{A}_{hid}^{boost}$ and its corresponding attraction basin $\mathcal{B}_{hid}^{boost}$ are shifted, the nonlinear dynamics of the system will keep unchanged.

Figure 7 plots the phase portraits and time sequences of the system (2) and the offset-boosted system (15), in which two sets of ICs (0, 0, 1) and (0, 0, 0) are respectively applied to the two systems and generate chaotic trajectories marked by cyan and magenta. Figure 7(a), (b), and (c) exhibit the phase portraits of the generated hidden chaotic attractors. Figure 7(d) shows the time sequences of the variable z. The results indicate that the attractor of the seed system (2) is successfully linearly boosted along the z direction with the amplitude 1. Since the basin $\mathcal{B}_{hid}^{boost}$ is intersected with the origin, therefore, we are able to observe the hidden chaotic attractor in hardware experiment via configuring a set of near-zero initial voltages for the capacitors.

4.2. Simulation and experiment

Based on the system equations in (15), by applying Kirchhoff laws, the corresponding analog circuit using common discrete circuit components can be further designed to verify the system's dynamical behaviours [47]. Figure 8 shows the complete circuit in Pspice simulation environment, in which the voltage-mode op-amps

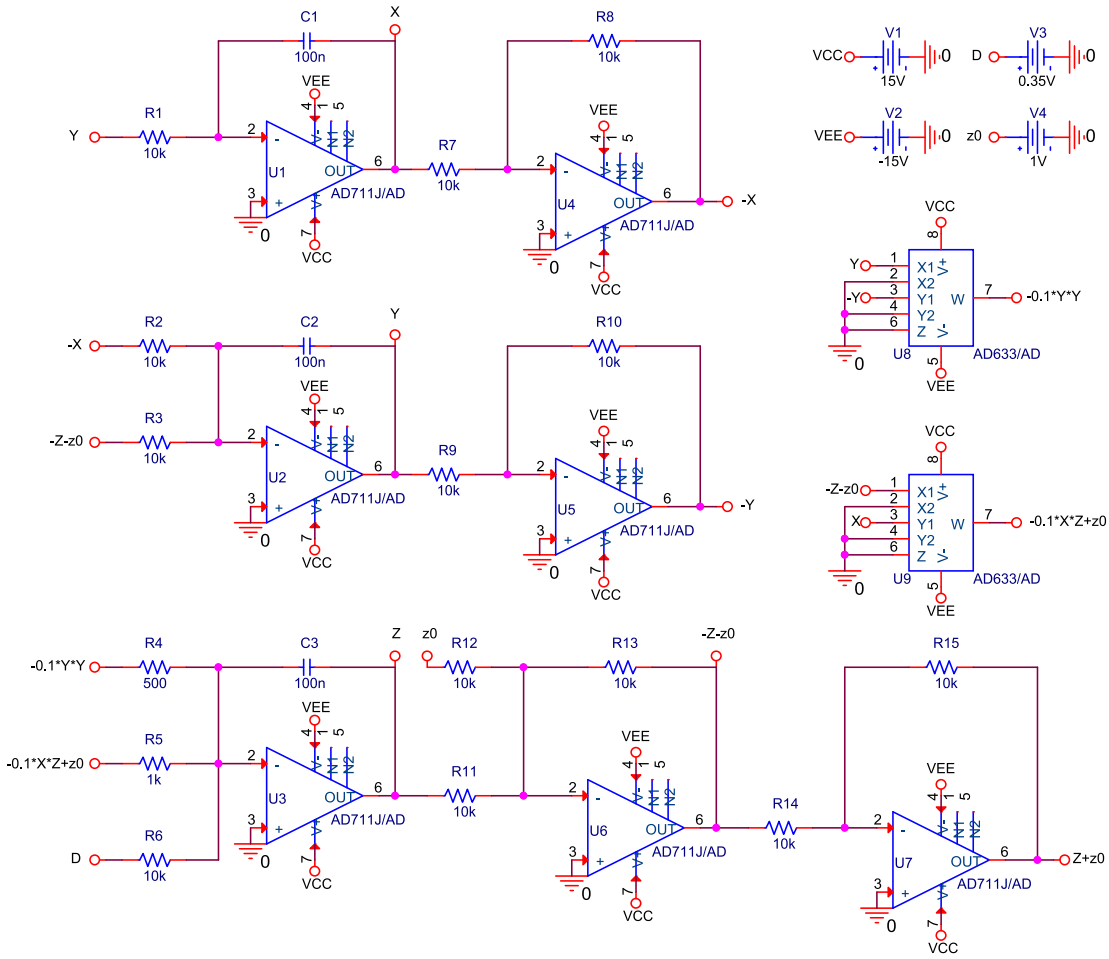

Figure 8. Circuit implementation of system (15) in Pspice.

(AD711JN) and multipliers (AD633JN) with 15 V direct-current voltage supplies are used. The op-amp-based resistor-capacitor integrator are used for inverse operation of the ODE system.

The circuit equations of figure 8 can be obtained as

$$\begin{cases} RC\dfrac{\mathrm{d}X}{\mathrm{d}t} = -\dfrac{R}{R_1}Y, \\ RC\dfrac{\mathrm{d}Y}{\mathrm{d}t} = \dfrac{R}{R_2}X + \dfrac{R}{R_3}(Z + z_0), \\ RC\dfrac{\mathrm{d}Z}{\mathrm{d}t} = \dfrac{R}{R_4}(g_1Y^2) + \dfrac{R}{R_5}(g_2X(Z + z_0)) - \dfrac{R}{R_6}D, \end{cases} \tag{16}$$

where $\frac{g_1R}{R_4} = a$, $\frac{R}{R_2} = c$, $\frac{R}{R_6}D = d$, g_1 and g_2 are two multiplier coefficients of AD633JN multipliers and is set as 0.1. Thus, $R_4 = gR/a = 500\ \Omega$, $R_2 = R/c = 10\ \mathrm{k}\Omega$, and $R_5 = gR = 1\ \mathrm{k}\Omega$. With this configuration, the circuit implementations are simplified and the unexpected situation of output saturation can be effectively avoided.

In equation (16), C and R are two generalized integrator factors and are used for the time scaling between the physical and the mathematical one, i.e., $t = \tau RC$. Here, $C = 100$ nF and $R = 10\ \mathrm{k}\Omega$ are used. Three output voltages of the integrating capacitors C_1, C_2, and C_3 are marked as X, Y, and Z, respectively; z_0 is a direct-current offset voltage and is set as 1 V; $R_1 \sim R_6$ are scaling resistors and $R_1 = R_2 = R_3 = R_6 = R = 10\ \mathrm{k}\Omega$, $R_4 = gR/a = 500\ \Omega$, and $R_5 = gR = 1\ \mathrm{k}\Omega$ (more detailed parameter configurations can be seen in figure 8). Under the following interactive simulation configuration in Pspice environment: 'Run to time: 1 s', 'Maximum step size: 1e-005', and 'Initial conditions: Set to zero', the output phase portraits of the circuit are shown in figure 9.

Based on the implemented circuit, the tested result from a hardware platform is shown in figures 10 and 11. It can be observed that the circuit simulated and physically tested results have good consistence with the

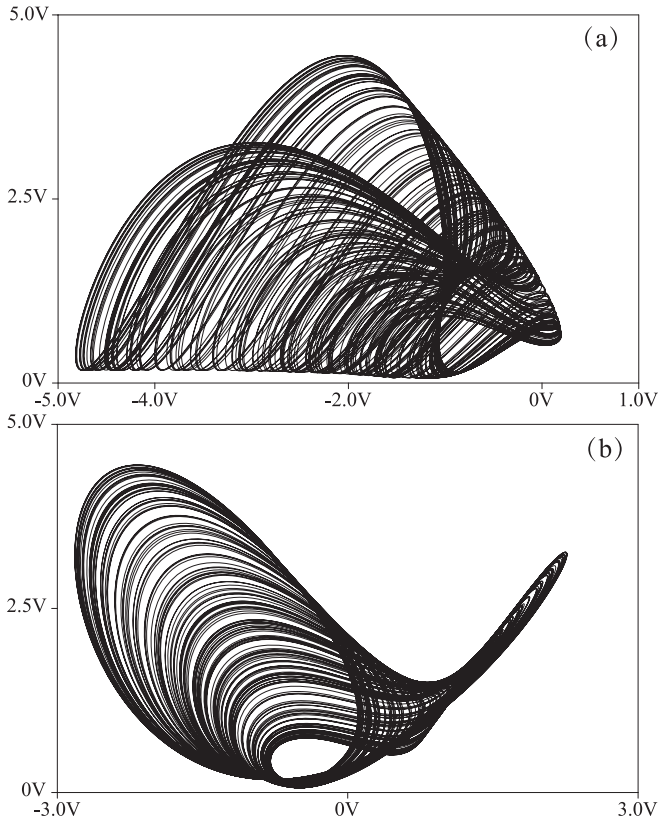

Figure 9. Circuit simulated phase portraits in two projection planes, where the typical parameters in figure 8 are used: (a) hidden chaotic attractor in the *Xvs.* $Z + z_0$ plane; (b) hidden chaotic attractor in the *Yvs.* $Z + z_0$ plane.

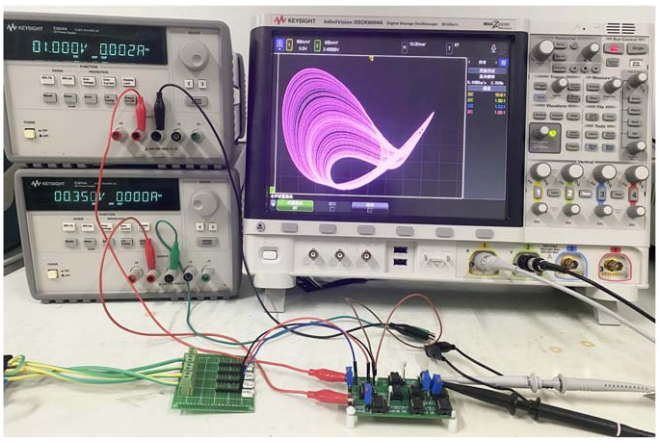

Figure 10. Hardware test platform with a measured chaotic phase portrait.

numerical results of figure 7, which confirmed the feasibility in experimental validation of the hidden chaotic attractor.

5. Conclusion

In this paper, we studied the nonlinear dynamics of a Chameleon chaotic system. It was shown that the system has different numbers of equilibria or has no equilibrium under different parameter configurations. Its complex self-excited and hidden oscillations were investigated via parameter-related bifurcations. Aided by computation simulation, we demonstrated the graphic structures of bifurcations under two-parameter variation. The results indicated that the chaotic region can be coined via period-doubling bifurcation route. Besides, the boundary

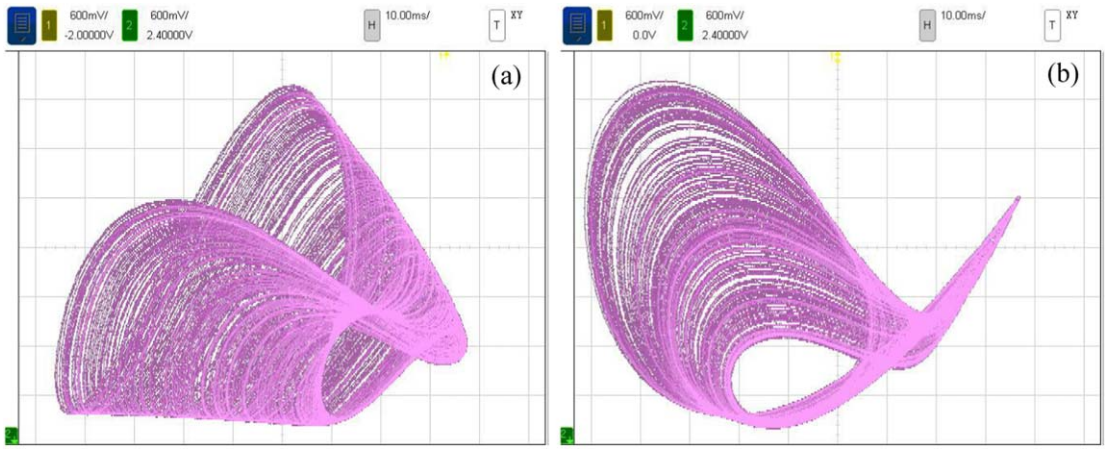

Figure 11. Experimentally captured phase portraits, where the typical circuit parameters in figure 8 are used: (a) measured result in the *Xvs.* $Z + z_0$ plane; (b) measured result in the *Yvs.* $Z + z_0$ plane.

between the unbounded area and bounded ones were clearly investigated, which provided an intuitive guidance for configuring the system parameters to obtain distinct self-excited and hidden attractors. In addition, the attraction basins of the hidden attractor were not associated with the origin, which made it difficult to be numerically localized and experimentally observed. We further applied the offset control scheme to make the basin of attraction intersect with the origin, thus effectively validated such hidden attractor in analog circuit experiment.

Acknowledgments

This work was supported by the National Natural Science Foundation of China (Grant No. 52 307 002 and 12 172 066); the Natural Science Foundation of Jiangsu Province, China (Grant No. BK20230628); the Scientific Research Foundation of Jiangsu Provincial Education Department, China (Grant No. 23KJB120002); the Project 333 of Jiangsu Province; and the College Student Innovation and Entrepreneurship Training Program of Changzhou University (Grant No. 202 310 292 376B).

Data availability statement

The data cannot be made publicly available upon publication because no suitable repository exists for hosting data in this field of study. The data that support the findings of this study are available upon reasonable request from the authors.

Conflicts of interest

The authors declare that there is no conflict of interest regarding the publication of this paper.

ORCID iDs

Ning Wang https://orcid.org/0000-0002-4453-8588
Quan Xu https://orcid.org/0000-0002-0370-9141

References

[1] Gomes I, Korneta W, Stavrinides S G, Picos R and Chua L O 2023 *Chaos Solitons Fractals* **166** 112927
[2] Wei Z, Zhu B, Yang J, Perc M and Slavinec M 2019 *Appl. Math. Comput.* **347** 265–81
[3] Wei Z, Wang F, Li H and Zhang W 2022 *Discret. Contin. Dyn. Syst. Ser. B* **27** 5029–45
[4] Fozin T F, Nzoko B K, Telem N A K, Njitacke Z T, Mouelas A A N and Kengne J 2022 *Phys. Scr.* **97** 075204
[5] Xu Q, Liu T, Ding S, Bao H, Li Z and Chen B 2023 *Cogn Neurodyn* **17** 755–66
[6] Oresanya B O, Si G, Xu X, Gong J and Guo Z 2023 *Phys. Scr.* **98** 115213
[7] Chua L O, Komuro M and Matsumoto T 1986 IEEE Trans *Circuits Syst.* **33** 1072–118
[8] Wang N, Li C, Bao H, Chen M and Bao B 2019 IEEE Trans. Circuits Syst. *I, Reg. Papers* **66** 4767–79

[9] Tchiedjo S K, Kenmoe G D and Kengne J 2023 *Phys. Scr.* **98** 105209
[10] Lorenz E N 1963 *J .Atmos. Sci.* **20** 130–41
[11] Wang H H, Sun K H and He S B 2015 *Phys. Scr.* **90** 015206
[12] Ahmadi A, Parthasarathy S, Natiq H, Rajagopal K, Huerta-Cuellar G and Jafari S 2023 *Phys. Scr.* **98** 055219
[13] Wang N, Xu D, Li Z and Xu Q 2023 *Chaos Solitons Fractals* **177** 114233
[14] Xu Q, Wang Y, Chen B, Li Z and Wang N 2023 *Chaos Solitons Fractals* **172** 113627
[15] Zhang S, Li C, Zheng J, Wang X, Zeng Z and Peng X 2022 *IEEE Trans. Ind. Electon.* **69** 7202–12
[16] Leonov G A, Kuznetsov N V and Vagaitsev V I 2011 *Phys. Lett. A* **375** 2230–3
[17] Leonov G A, Kuznetsov N V and Vagaitsev V I 2012 *Physica. D* **241** 1482–6
[18] Leonov G A and Kuznetsov N V 2013 *Int. J. Bifur. Chaos.* **23** 1330002
[19] Jafari S, Sprott J C and Nazarimehr F 2015 *Eur. Phys. J. Special Topics* **224** 1469–76
[20] Kuznetsov N V, Leonov G A, Mokaev T N, Prasad A and Shrimali M D 2018 *Nonlinear Dyn.* **92** 267–85
[21] Wang N, Cui M, Yu X, Shan Y and Xu Q 2023 *Chaos Solitons Fractals* **177** 114242
[22] Dudkowski D, Jafari S, Kapitaniak T, Kuznetsov N V, Leonov G A and Prasad A 2016 *Phys. Rep.* **637** 1–50
[23] Ahmad I, Srisuchinwong B and Usman Jamil M 2023 *Int. J. Bifurcation Chaos* **33** 2330010
[24] Kuznetsov N V, Mokaev T N, Kuznetsova O A and Kudryashova E V 2020 *Nonlinear Dyn.* **102** 713–32
[25] Shatnawi M T, Abbes A, Ouannas A and Batiha I M 2023 *Phys. Scr.* **98** 035213
[26] Das P and Mandal S 2023 *Phys. Scr.* **98** 115252
[27] Li C, Sprott J C and Xing H 2016 *Phys. Lett. A* **380** 1172–7
[28] Li C, Wang X and Chen G 2017 *Nonlinear Dyn.* **90** 1335–41
[29] Pham V T, Jafari S, Vaidyanathan S, Volos C and Wang X 2016 *Science China Technological Sciences* **59** 358–63
[30] Yang Y, Huang L, Xiang J, Bao H and Li H 2021 *AEÜ-Int. J. Electron. Commun.* **135** 153710
[31] Sprott J C 1994 *Phys. Rev. E* **50** R647
[32] Wei Z 2011 *Phys. Lett. A* **376** 102–8
[33] Jafari S, Sprott J C and Golpayegani M R H 2013 *Phys. Lett. A* **377** 699–702
[34] Tahir F R, Jafari S, Pham V P, Volos C and Wang X 2015 *Int. J. Bifurcation Chaos* **25** 1550056
[35] Hu X, Liu C, Liu L, Ni J and Li S 2016 *Nonlinear Dyn.* **86** 1725–34
[36] Wang N, Zhang G, Kuznetsov N and Li H 2022 *Commun Nonlinear Sci. Numer Simul* **107** 106194
[37] Jafari M A, Mliki E, Akgul A, Pham V T, Kingni S T, Wang X and Jafari S 2017 *Nonlinear Dyn.* **88** 2303–17
[38] Mobayen 2018 *Nonlinear Dyn.* **92** 1539–53
[39] Sprott J C 2011 *Int. J. Bifur. Chaos* **21** 2391–4
[40] Sprott J C and Munmuangsaen B 2018 *Chaos Solitons Fractals* **113** 261–2
[41] Minati L 2021 *Chaos Solitons Fractals* **144** 110656
[42] Yang Y, Huang L, Kuznetsov N, Chai B and Guo Q 2024 *IEEE Trans. Ind. Electron.* **71** 3986–95
[43] Wang N, Xu D, Kuznetsov N, Bao H, Chen M and Xu Q 2023 *Chaos Solitons Fractals* **170** 113427
[44] Yang Y, Huang L, Kuznetsov N V and Lai Q 2023 *IEEE Trans Circuits Syst. I* (https://doi.org/10.1109/TCSI.2023.3312489)
[45] Wolf A, Swift J B, Swinney H L and Vastano J A 1985 *Phys. D* **16** 285–317
[46] Danca M F, Bourke P and Kuznetsov N V 2019 *Int. J. Bifur. Chaos* **29** 1930001
[47] Newcomb R W and El-Leithy N 1986 *Circuit Syst. Signal Process* **5** 321–41